Complete phase diagram for three-band Hubbard model with orbital degeneracy lifted by crystal field splitting

Li Huang,[1,2] Liang Du,[1] and Xi Dai[1]

[1]*Beijing National Laboratory for Condensed Matter Physics and Institute of Physics, Chinese Academy of Sciences, Beijing 100190, China*

[2]*Science and Technology on Surface Physics and Chemistry Laboratory, P.O. Box 718-35, Mianyang 621907, Sichuan, China*

(Received 22 March 2012; revised manuscript received 13 July 2012; published 30 July 2012)

Motivated by the unexplored complexity of the phase diagrams for multiorbital Hubbard models, a three-band Hubbard model at integer fillings ($N = 4$) with orbital degeneracy lifted partially by crystal field splitting is analyzed systematically in this work. By using the single-site dynamical mean-field theory and rotationally invariant Gutzwiller approximation, we have computed the full phase diagram with Coulomb interaction strength U and crystal field splitting Δ. We find a large region in the phase diagram where an orbital-selective Mott phase will be stabilized by the positive crystal field lifting the orbital degeneracy. Further analysis indicates that Hund's rule coupling is essential for the orbital-selective Mott phase, and the transition toward this phase is accompanied by a high-spin to low-spin transition. Such a model may be relevant for the recently discovered Ru-based materials.

DOI: 10.1103/PhysRevB.86.035150 PACS number(s): 71.10.Fd, 71.28.+d, 71.30.+h

I. INTRODUCTION

The Mott-Hubbard metal-insulator transition (MIT) has been a subject of great interest for decades.[1] Most of the attention before this century has been focused on the one-band case only because most of the qualitative features of MIT have already been captured by the single-band Hubbard model, as shown by numerous studies using the single-site dynamical mean-field theory (DMFT).[2] However, in realistic materials most of the Mott transitions involve more than one band and thus exhibit multiorbital features.[3] Multiorbital extension of the Hubbard model allows more realistic description of MIT and other strongly correlated physics, which contains, in general, much richer phase diagrams and exotic physical phenomena. For instance, the redistribution of electrons among different orbitals leads to new scenarios, such as orbital ordering,[4] high-spin to low-spin (HS-LS) transition,[5] orbital-selective Mott transition (OSMT),[6] etc.

Mott transitions in multiorbital models have been studied within the framework of DMFT for more than ten years.[2,7] Previous studies show[8] that simply increasing the band degeneracy only changes the critical interaction strength U_c but does not change the fundamental features of Mott transition, where all the degenerate bands undergo Mott transition simultaneously under the increment of interaction strength. Recent studies of realistic materials have focused interest on the interplay between MIT and orbital degeneracy.[6,9–11] A very fundamental question raised in this field is how the multiorbital systems respond to the breakdown of the orbital degeneracy. In such a system, it is possible that the Mott transitions in different orbitals happen separately, which is the so-called OSMT and was suggested first by Anisimov *et al.*[6] in the pioneering study of $Ca_{2-x}Sr_xRuO_4$.

After its proposal, the concept of OSMT attracted much scientific interest.[12–25] The early DMFT studies on this problem were focused on the two-band Hubbard model with half-filling, which is the simplest system that might have OSMT when the bandwidths of the two bands are different. The DMFT calculations from different groups with finite-temperature exact diagonalization[12,13] and the Hirsch-Fye quantum Monte Carlo method[14–18] as impurity solvers converge to two essential conclusions: (1) The OSMT in the two-band Hubbard model is mainly induced by the bandwidth difference, which breaks the degeneracy between the two bands, and the crystal field splitting plays a minor role here. (2) The emergence of OSMT is very sensitive to the symmetry of the local interaction. In other words, OSMT easily occurs when the local interaction is rotationally invariant but not when the local interaction breaks the rotational invariance.

The OSMT in the three-band Hubbard model, which is more relevant to the realistic situation of $Ca_{2-x}Sr_xRuO_4$,[6,22] is not a trivial generalization of the two-band model. In two-band systems, the OSMT can only take place in the half-filling case, while in three-band systems it can take place when the occupation numbers are 2, 3, or 4 or even for fractional occupation.[20,23] When the total occupation number is 3, the three-band system is half-filled, and actually, the situation is very similar to the two-band model. The most interesting case is when the occupation number is 2 or 4, which can be transformed between each other by the particle-hole symmetry. Recently, de' Medici *et al.*[23] proposed a new mechanism for OSMT, which happens in three-band systems with a filling factor of 2 or 4. In this new scenario of OSMT, the driving force is not the difference of the bandwidth but the crystal field splitting lifting the band degeneracy. Then Kita *et al.*[26] investigated how the orbital level splitting and Ising-type Hund's rule coupling affect the Mott transition in the case of two electrons per site. Their results reveal that the critical interaction strength separating a metallic phase and two kinds of insulating phases shows a nonmonotonic behavior as a function of the orbital level splitting. They suggested that this behavior is characteristic for 1/3 filling, in comparison with the preceding results for different fillings and for two-band models. It is worth noting that the three-band system is very popular in transition-metal compounds.[1,3] Provided the Fermi energy falls into the t_{2g} bands, the tetragonal distortion

will further split them into a nondegenerate a_{1g} band and twofold-degenerate e'_g bands. When the occupation number is 4, the appropriate crystal field will redistribute the four electrons into a_{1g} band and e'_g bands as 1 and 3, respectively [dubbed the (3,1) configuration]. Thus, if we neglect the correlation between a_{1g} and e'_g subsystems, the a_{1g} band becomes a one-band system with half-filling, and e'_g bands become a two-band system with quarter-filling, which will lead to an orbital-selective Mott phase (OSMP) at equal bandwidth because it is much easier to get a Mott insulator in the a_{1g} band. The mean-field phase diagram of this model determined by the slave-spin method[23,24] contains quite a large region for OSMP, in which the a_{1g} band has already become a Mott insulator while the e'_g bands are still metallic.

The OSMT driven by the band degeneracy lifting is quite a robust phenomenon determined by the interplay between crystal symmetry and correlation effects. In a previous work,[23] the phase diagram of the three-band Hubbard model was mainly calculated by the slave-spin method, which is qualitatively correct but not accurate enough. In the present paper, we study systematically this t_{2g}-like Hubbard model with crystal field splitting by two more accurate methods: the DMFT method combined with a state-of-the-art hybridization expansion continuous-time quantum Monte Carlo impurity solver (generally abbreviated as DMFT + CT-HYB)[27–30] and the newly developed rotationally invariant Gutzwiller approximation (RIGA) method.[31–34] The metal-insulator phase diagram, band-specific quasiparticle weight Z_a, orbital occupation number n_a, and local magnetic moment $M_{\rm eff}$ are computed by both methods with respect to crystal field splitting Δ and Coulomb interaction strength U. Based on these results, we mainly discuss three important aspects of OSMT in this system: (i) the crucial role of Hund's rule coupling, (ii) the redistribution of four electrons among the a_{1g} and e'_g bands, and (iii) the relationship between OSMT and HS-LS spin-state crossover.

The rest of this paper is organized as follows: In Sec. II the three-band Hubbard model treated in this work is specified. In Sec. III A the main results of this paper, U-Δ phase diagrams for rotationally invariant interaction and SU(N) density-density interaction, are presented and compared with each other. In Sec. III B, the redistribution of electrons among different orbitals and its relationship with the OSMT are discussed in detail. And the accompanying HS-LS spin-state crossovers are discussed in Sec. III C. Section IV serves as a conclusion.

II. MODEL

We consider the three-band Hubbard model defined by

$$H = -\sum_{ij,a\sigma} t_{ij} c^{\dagger}_{ia\sigma} c_{ja\sigma} + \sum_i H^i_{\rm loc}, \tag{1}$$

where $c^{(\dagger)}_{ia\sigma}$ is an annihilation (creation) operator of an electron with spin σ ($=\uparrow,\downarrow$) and orbital a ($=1,2,3$) at the ith site and t_{ij} is the hopping integral between site i and site j. The local part of Hamiltonian $H^i_{\rm loc}$ can be defined as follows (for the sake of simplicity, the site index i has been ignored in the rest of this paper):

$$\begin{aligned} H_{\rm loc} = &-\sum_{a\sigma}(\mu-\Delta_a)n_{a\sigma} + \sum_a U n_{a\uparrow}n_{a\downarrow} \\ &+ \sum_{a>b,\sigma}[U' n_{a\sigma}n_{b\bar{\sigma}} + (U'-J)n_{a\sigma}n_{b\sigma}] \\ &- \sum_{a<b} J(d^{\dagger}_{a\downarrow}d^{\dagger}_{b\uparrow}d_{b\downarrow}d_{a\uparrow} + d^{\dagger}_{b\uparrow}d^{\dagger}_{b\downarrow}d_{a\uparrow}d_{a\downarrow} + \text{H.c.}). \end{aligned} \tag{2}$$

Here $n_{a\sigma} = c^{\dagger}_{a\sigma}c_{a\sigma}$ is the number operator, μ is the chemical potential, and Δ_a is the energy level for orbital a. In the interaction terms, U (U') is the intraorbital (interorbital) Coulomb interaction, and J is the Hund's rule coupling. The constrained condition $U = U' + 2J$ is imposed as usual, which is valid for atomic-like local orbitals. The above interaction terms include both the spin-flip and pair-hopping terms and thus are rotationally invariant in the spin space. In order to elucidate the Mott MIT in the case of four electrons per site, the chemical potential μ is adjusted dynamically in the simulations to fix the electron filling per site as $N = 4$. In the present paper, we focus on the t_{2g}-like bands under the tetragonal crystal field, which are split into the nondegenerate a_{1g} band (namely, orbital 1) and doubly degenerate e'_g bands (namely, orbitals 2 and 3), as mentioned above. Therefore the on-site energy level is assumed to be $\Delta_1 \neq \Delta_2 = \Delta_3$, and their difference is defined as $\Delta = \Delta_1 - \Delta_2$.

This lattice model [see Eqs. (1) and (2)] can be solved in the framework of single-site DMFT,[2,7] which neglects the momentum dependence of the self-energy and reduces the original lattice problem to the self-consistent solution of an effective impurity model. In this paper, a semicircular density of states with half bandwidth $D = 1$ is used, which corresponds to the infinite coordination Bethe lattice. All the orbitals have equal bandwidth, and the energy unit is set to be D. To solve the effective impurity model, the CT-HYB impurity solver within general formulation[27–30] is adopted. This method allows us to access the strong interaction regime down to very low temperatures. In our calculations, the system temperature is set to be $T = 0.01$ (corresponding to inverse temperature $\beta = 100$) unless otherwise stated. In each DMFT iteration, typically 4×10^8 Monte Carlo samplings have been performed to reach sufficient numerical accuracy.

In the present work, we also use the efficient RIGA method[31–34] to crosscheck the results obtained by the DMFT + CT-HYB method. In contrast to the finite-temperature DMFT + CT-HYB calculations, only the zero-temperature physical quantities can be obtained by using the RIGA method. Although the RIGA method cannot access the dynamical properties of correlated systems, it provides a very fast and economic way to calculate the ground-state properties, for example, the total energy and occupation numbers. Thus, it can be viewed as a good complementary approach to the DMFT + CT-HYB method. As will be discussed in detail in the following sections, the phase diagrams and other physical properties obtained by both methods are in very good agreement. The presence of both results from the two different methods gives a more comprehensive description of the phase diagrams for both zero and finite temperatures.

The implementation details of the RIGA method have been presented elsewhere.[34]

III. RESULTS AND DISCUSSION

A. U-Δ phase diagram

To map out the metal-insulator phase diagram we have computed thoroughly the dependence of charge density, quasiparticle weight, and local magnetic moment as a function of crystal field splitting for various Coulomb interaction strengths. In this section, we will focus first on the U-Δ phase diagrams with both nonzero and zeroed Hund's rule coupling J. We will show in the following that the Ising-type Hund's rule coupling J_z is extremely crucial for the appearance of OSMP in the three-band system with four electrons.

When the spin-flip and pair-hopping interaction terms are taken into full consideration, the Hamiltonian for the three-band Hubbard model is rotationally invariant in the spin space, and the phase diagram contains four different phases, which are the metal, band insulator, OSMP, and Mott insulator phases, respectively. The obtained U-Δ phase diagrams for the $J = U/4$ case are illustrated in Fig. 1. The top panel is the results obtained by the DMFT + CT-HYB method, and the bottom panel is obtained by the RIGA method. From Fig. 1, we can easily see that the consistency between both methods is quite excellent, except the phase boundary obtained by the RIGA method is a bit higher, which is similar to the situations found in the one- and two-band models.[33,34] Comparing with the analogous phase diagrams previously obtained by the slave-spin method,[23,24] there are two important differences. First, the critical U_c for Mott transition at $\Delta = 0$ is much lower in the phase diagram determined by the DMFT + CT-HYB method. Second, in the phase diagrams obtained with both the DMFT + CT-HYB and RIGA methods, the phase boundary between the metal and band insulator phases depends on U monotonically; however, in the phase diagram obtained with the slave-spin method, it decreases first and then increases.[23] This difference is mainly due to the oversimplified treatment of Hund's rule coupling terms in the slave-spin method.[24]

The general shape of the phase diagram can be easily understood by considering two limiting cases: (i) For $\Delta = 0$, the model reduces to a fully degenerate three-band Hubbard model with total filling $N = 4$, which undergoes a Mott transition around $U = 10.0$. (ii) For the uncorrelated limit (i.e., $U = 0$), when $\Delta > 0$ a simple transition from metal to band insulator can be observed at $\Delta = 2.0$ with the fully occupied e'_g bands and empty a_{1g} band. Another transition can also be seen on the negative side at $\Delta = -1.0$, after which the nondegenerate a_{1g} band is a fully occupied band insulator and the doubly degenerate e'_g bands are metallic at half-filling.

When both the Coulomb interaction U and crystal field Δ are finite, the phase diagram is quite complicated and very different for $\Delta > 0$ and $\Delta < 0$. Now let's have a further discussion about this phase diagram. On one hand, if the crystal field splitting $\Delta > 0$, the isolate a_{1g} band is lifted up, and the doubly degenerate e'_g bands are pushed down. This part of the phase diagram can be divided vertically into two regions: (i) For $2.0 > \Delta > 0.0$, the system undergoes successive transitions from metal to Mott insulator through an OSMP as the Coulomb interaction strength increases. (ii) For $\Delta > 2.0$, the system undergoes a different type of successive transitions from band insulator to Mott insulator through metal and OSMP phases in sequence. On the other hand, if the crystal field splitting $\Delta < 0$, i.e., the a_{1g} band is lower than the twofold-degenerate e'_g bands, this part of the phase diagram can be divided vertically into three different regions: (i) For $-1.0 < \Delta < 0.0$, with weak Coulomb interaction both bands have fractional filling and are metallic. As the Coulomb interaction strength U increases, the system undergoes a transition from a fully metallic phase to an insulator phase, after which the occupation numbers for both the a_{1g} and e'_g bands are 2. Since the a_{1g} band has no degeneracy, it is completely occupied and becomes

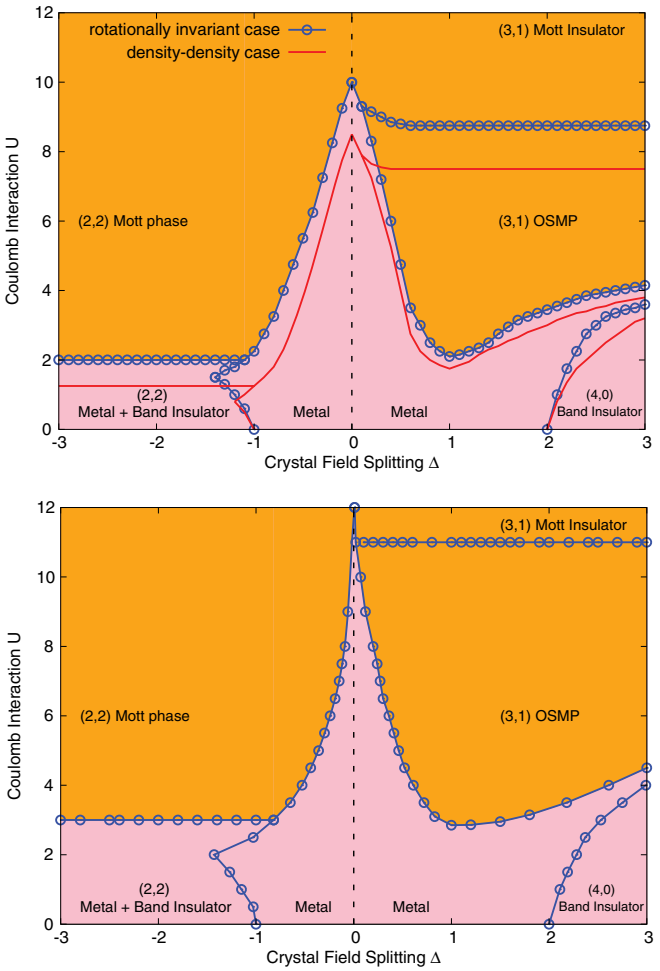

FIG. 1. (Color online) Calculated phase diagrams of the three-band Hubbard model with rotationally invariant interactions in the plane of Coulomb interaction U ($J = U/4$) and crystal field splitting Δ ($\Delta = \Delta_1 - \Delta_2$). (top) Calculated by the DMFT + CT-HYB method[27,28] at finite temperature $T = 0.01$. (bottom) Calculated by the RIGA method[34] at zero temperature. In all the calculations, the chemical potential μ is adjusted dynamically to fulfill the total occupation number condition ($N = 4$). The label "(2,2) Metal + Band Insulator" means the twofold-degenerate bands (e'_g states) are metallic while the nondegenerate band (a_{1g} state) is insulating, and (2,2) means the corresponding orbital occupancies. All the other labels have similar explanations. The pink zone shows the LS state, and the orange zone shows the HS state. The solid blue line with circles and solid red line denote the phase boundaries for rotationally invariant interaction and Ising-type Hund's rule coupling cases, respectively.

a band insulator in this situation. At the same time the e'_g bands with double degeneracy become Mott insulators with half-filling. Thus, it is called the (2,2) Mott insulator phase throughout this paper. (ii) For $-1.4 < \Delta < -1.0$, with weak Coulomb interaction the a_{1g} band is already fully occupied, and the e'_g bands are half-filled and metallic. As the Coulomb interaction strength U increases, the system first becomes a fully metallic phase with fractional filling factors for all the bands and then goes back to the original (2,2) metal plus band insulator phase after a "reentrance" transition. Finally, it becomes the (2,2) Mott insulator phase once $U > 2.0$. (iii) For $\Delta < -1.4$, the a_{1g} band remains fully occupied regardless of the interaction strength, and the system reduces to an equivalent two-band model with half-filling, which undergoes a typical Mott MIT around $U = 2.0$, as determined by the DMFT + CT-HYB method. As seen in Fig. 1, the OSMP covers a wide parameter range. In a previous work, de' Medici *et al.* have suggested that the non-Fermi-liquid properties can be seen in the OSMP.[23] Not surprisingly, in the present work the non-Fermi-liquid behavior is also observed in the OSMP determined by the DMFT + CT-HYB method. The imaginary part of the calculated low-frequency Matsubara self-energy function (only for the itinerant component of OSMP), $\mathrm{Im}\Sigma(i\omega)$, exhibits apparently fractional power-law behavior with respect to $i\omega$, which is the signature of the non-Fermi-liquid phase. The non-Fermi-liquid behavior in OSMP was first proposed by de' Medici *et al.*[23] with the DMFT + ED method and was confirmed by our DMFT + CT-HYB studies.

We note that the Coulomb interaction U has two basic effects for multiorbital systems. One is to reduce the quasiparticle weight;[12–15] the other one is to redistribute the electrons among different bands.[5,20,24] The interplay between these two effects determines the schematic structure of the above phase diagrams. Next we will focus on the first effect, and then the second effect will be discussed in detail in the following sections. The band-specific quasiparticle weights Z_a as a function of Coulomb interaction U are shown in Fig. 2(a). The crystal field splitting is fixed to $\Delta = 1.0$. For simplicity, only the results obtained with the RIGA method, which are consistent with those obtained with the DMFT + CT-HYB method, are displayed in Fig. 2(a). It is apparent that the quasiparticle weights Z_a decrease monotonously from 1.0 to 0.0 when Coulomb interaction strength increases. As $U < 3.0$, the Z_a are larger than 0.1, and both the e'_g and a_{1g} bands are metallic. As $U > 3.0$, Z_1 becomes zero, while $Z_2(=Z_3)$ is still considerable. This means that the a_{1g} band undergoes a Mott MIT and turns into an insulator around $U = 3.0$, and at the same time the e'_g bands remain metallic, which is the so-called (3,1) OSMP. When the Coulomb interaction strength continues to increase ($U > 11.0$ for the RIGA method and $U > 9.0$ for the DMFT + CT-HYB method), the e'_g bands undergo another Mott MIT, and the system goes to the (3,1) Mott insulator phase finally; then all Z_a will approach zero. Indeed, the quasiparticle weights are used to determine the phase-transition points for the RIGA calculations. Since Z is not a well-defined quantity in finite temperatures any longer, with respect to the DMFT + CT-HYB method, alternative quantities such as the $G(\beta/2)$, orbital occupation, and kinetic energy are used to determine the phase boundaries. Particularly, the imaginary-time Green's function at $\tau = \beta/2$ represents the integrated

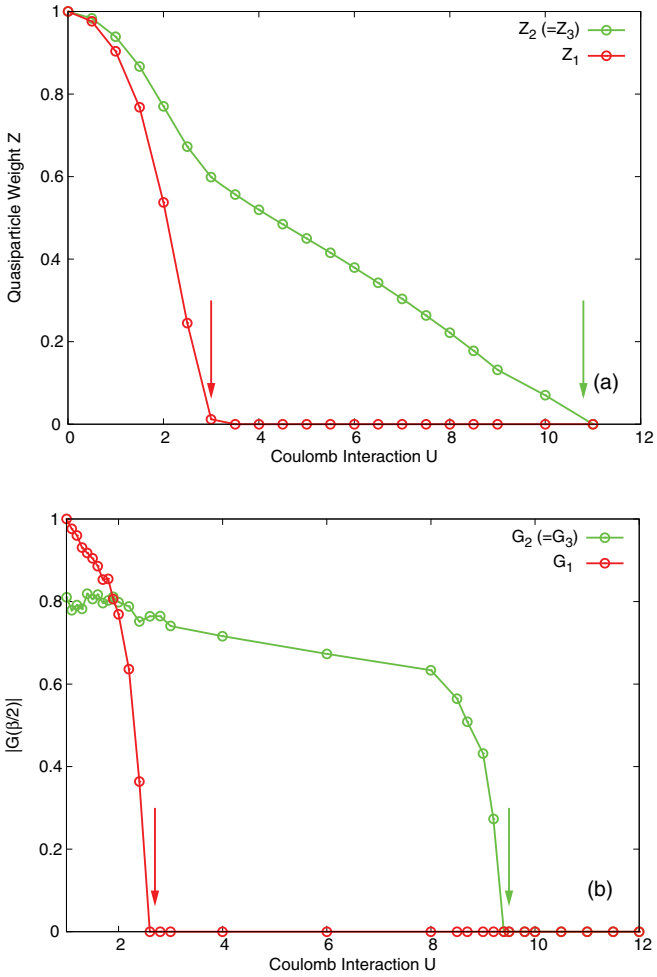

FIG. 2. (Color online) (a) Quasiparticle weights Z_a as a function of Coulomb interaction U for selected crystal field splitting $\Delta = 1.0$. The calculations are done by the RIGA method at zero temperature.[34] The colored arrows correspond to metal-insulator transition points. (b) The U-dependent imaginary-time Green's function at $\tau = \beta/2$ for $\Delta = 1.0$. The calculations are done by the DMFT + CT-HYB method at $\beta = 100$. In this plot, the quantities renormalized by $G(\beta/2)|_{U=1.0}$ for the a_{1g} band (orbital 1) are shown, and the colored arrows correspond to phase-transition points as well.

spectral weight within a few k_BT of the Fermi level, so it is a reasonable physical quantity to discuss the metal-insulator transition as well.[14] In Fig. 2(b) $G(\beta/2)$ as a function of Coulomb interaction U for selected crystal field splitting $\Delta = 1.0$ is plotted. It is apparent that the phase-transition points determined by the two methods accord with each other to some extent. As pointed out in previous works,[12,26] the OSMTs are of the first order at finite temperatures. In Fig. 2 we observe sudden drops for Z_a and $G(\beta/2)$ around the phase-transition points, which correspond to typical first-order transitions.

The Hund's rule coupling J has enormous influence on the metal-insulator phase diagram for the multiorbital Hubbard model.[26,35] It is noted that if we neglect the spin-flip and pair-hopping terms, only keeping the Ising-type Hund's rule coupling term J_z $(=J)$, we can obtain a very similar phase diagram, albeit the phase boundary is shifted downwards

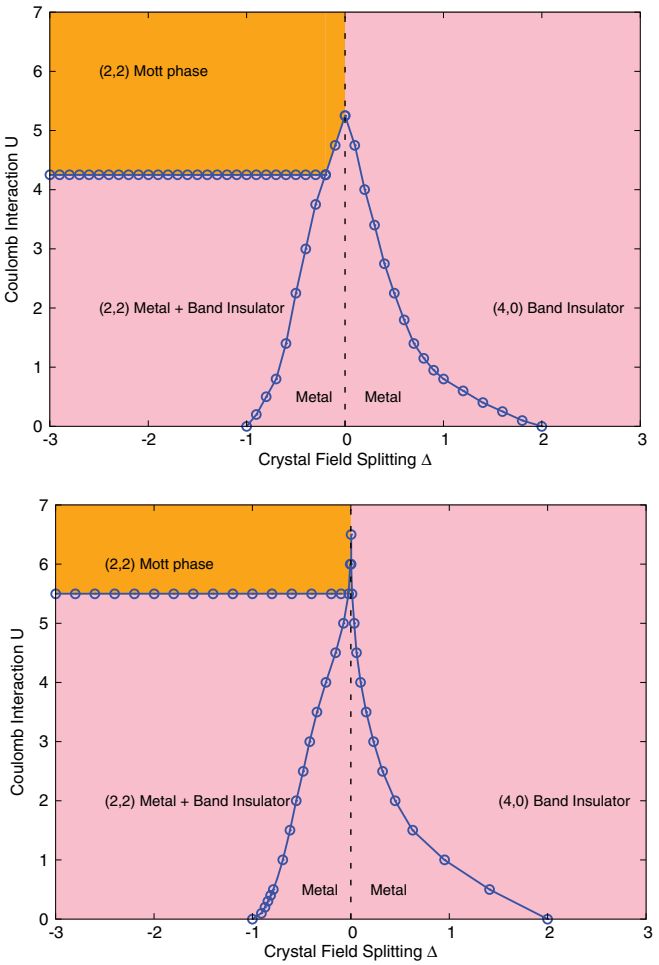

FIG. 3. (Color online) Calculated phase diagrams of the three-band Hubbard model with SU(N) density-density interaction in the plane of Coulomb interaction U ($J = 0.0$) and crystal field splitting Δ ($\Delta = \Delta_1 - \Delta_2$). (Top) Calculated by the DMFT + CT-HYB method[27,28] at finite temperature $T = 0.01$. (Bottom) Calculated by the RIGA method[34] at zero temperature. IN the calculations, the chemical potential μ is adjusted dynamically to fulfill the total occupation number condition ($N = 4$). With respect to the explanations of labels and colored zones in this figure, please refer to the caption of Fig. 1 and main text.

slightly (see the red lines in Fig. 1). It is apparent that the Ising-type Hund's rule coupling term J_z is the key requirement for OSMT and such a rich phase diagram. In order to reveal the underlying physics more clearly we also did calculations for the phase diagram of a similar three-band Hubbard model without any Hund's rule coupling terms ($J = 0$). Thus, we can compare the U-Δ phase diagrams for the cases with finite J (see Fig. 1) and SU(N) $J = 0$ (see Fig. 3). Obviously, the latter is much simpler and has no OSMP in the whole phase diagram. The top panel of Fig. 3 is the calculated results obtained by the DMFT + CT-HYB method, and the bottom panel of Fig. 3 is obtained by the RIGA method. These two methods give almost identical results again. First, we concentrate on the noninteraction case ($U = 0$). On one hand, when the crystal field splitting is positive ($\Delta > 0$), an obvious transition can be seen at $\Delta = 2.0$, after which the system becomes a band insulator. On the other hand, when the crystal field splitting is negative ($\Delta < 0$), a similar MIT can be found at $\Delta = -1.0$. When $\Delta > 0$, the phase diagram only consists of metal and band insulator phases. The lower left region is metallic, and the upper right region is a band insulator phase. The OSMP disappears completely. When $\Delta < 0$, the phase diagram contains metal, band insulator, and Mott insulator phases, but the characteristic "tip" which can be clearly seen around $U = 1.0$ and $\Delta = -1.2$ in Fig. 1 vanishes, and the phase boundary between the (2,2) metal plus band insulator and the (2,2) Mott insulator is shifted upward significantly. Thus, in summary the Hund's rule coupling J has played a key role in the phase diagram. More specifically, finite J_z is the minimal requirement to drive an OSMT.

B. Redistribution of electrons

In this section, we will discuss the second important effect of Coulomb interaction U on multiorbital systems with broken symmetry: the redistribution of electrons among different orbitals. In order to understand the intriguing physics contained in the U-Δ phase diagrams more clearly, we further plot the occupation numbers of the nondegenerate a_{1g} band as a function of Coulomb interaction U and crystal field splitting Δ in Figs. 4 and 5, respectively.

In Fig. 4(a), the evolution of the orbital occupancy with the Coulomb interaction strength is shown. The vertical arrows denote phase-transition points. In Fig. 4(a), only the orbital filling of the nondegenerate band (a_{1g} band) is plotted. For a negative crystal field, the a_{1g} band is much lower in energy, and the effect of the Coulomb interaction depends on the value of the crystal field Δ in the following way: (i) For $0 > \Delta > -1.0$, the effect of the correlation effect is to transfer electrons from the e'_g bands to the a_{1g} band until it is fully occupied and becomes a band insulator, as shown by the blue curve in Fig. 4(a). (ii) For $-1.0 > \Delta > -1.4$, the a_{1g} band is already fully occupied in the noninteracting case, and the effect of the correlation is nonmonotonic. With the increase of the repulsive interaction U and Hund's rule coupling J, the occupation number of the a_{1g} band first drops due to the Hund's rule coupling and then returns back to being fully occupied. We note that the interesting nonmonotonic behavior of the occupation is the consequence of the interplay between the Hund's rule coupling J, which favors an even distribution of the electrons, and the Coulomb repulsive interaction U, which tends to increase the occupation difference between orbitals. Therefore, this behavior disappears when the Hund's rule coupling has been set to zero, as shown in Fig. 4(b). (iii) For $\Delta < -1.4$, the charge distribution will not be affected by the correlation effect, and the occupation number of the a_{1g} band remains constant with the increase of U. While the situation is very different for $\Delta > 0$, in this case the energy level of the a_{1g} band is higher, and the occupation number is less than 0.5 in the noninteracting case. As we can see from Fig. 4(a), the increase of the interaction strength will pump the electrons from the e'_g bands to the a_{1g} band again until the latter reaches half-filling and becomes a Mott insulator. When the crystal field strength Δ is smaller than 2.0, all the bands are metallic, and the system becomes OSMP once the a_{1g} band reaches half-filling. However, when Δ is larger than 2.0, the system starts from a typical band insulator with fully

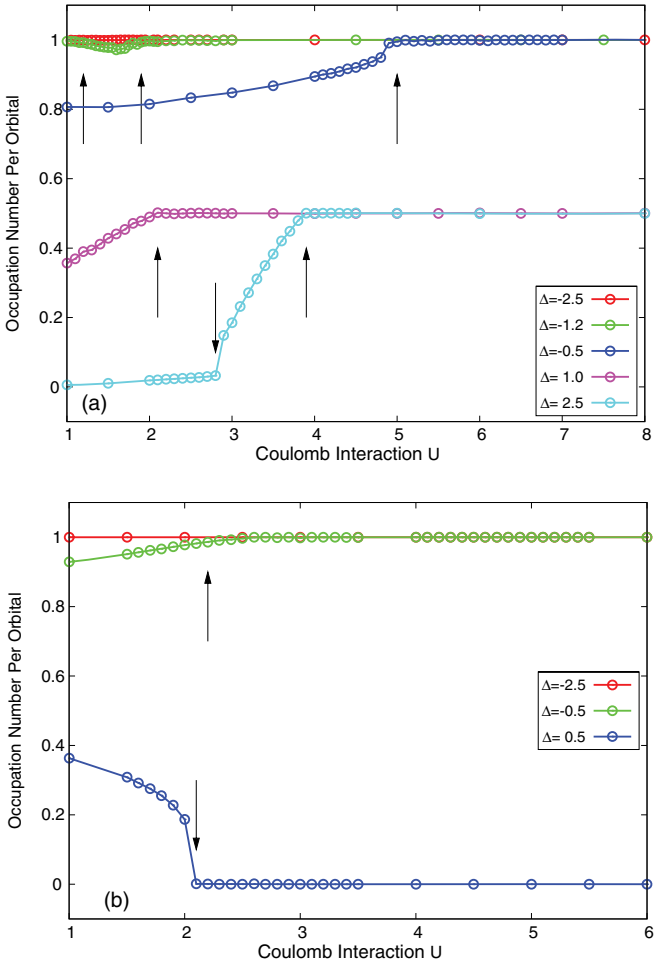

FIG. 4. (Color online) Orbital filling as a function of Coulomb interaction U for selected crystal field splitting Δ values. (a) Rotationally invariant interaction case. (b) SU(N) $J = 0$ case. The results are calculated with the DMFT + CT-HYB method[27,28] at finite temperature $T = 0.01$. Only the charge densities of the nondegenerate band (the a_{1g} band) are shown. The arrows correspond to possible phase-transition points.

occupied e'_g and empty a_{1g} bands. With the increase of the Coulomb interaction, it first becomes metallic when the a_{1g} band becomes partially populated and finally goes into the OSMP. Thus, there exist at least two phase-transition points in the $\Delta = 2.5$ curve.

In Figs. 5(a)–5(c), we plot the occupancy of the a_{1g} band under a fixed Coulomb interaction strength U as a function of crystal field splitting Δ. For weak Coulomb interaction ($U = 1.0$), when the crystal field splitting is increased from very negative to very positive values, two plateaus can be found in the occupancy of the a_{1g} band, which correspond to fully occupied and empty situations, respectively. The occupation numbers decrease smoothly between the two plateaus corresponding to the metallic phase. For an intermediate interaction strength ($U = 3.0$) with nonzero Hund's rule coupling J, there is an additional plateau with an occupancy that is half-filled, which corresponds to the OSMP, which is completely absent as long as $J = 0$. For a strong interaction strength ($U = 7.0$), in the second plateau, which corresponds to the OSMP as well, the a_{1g} band is half-filled.

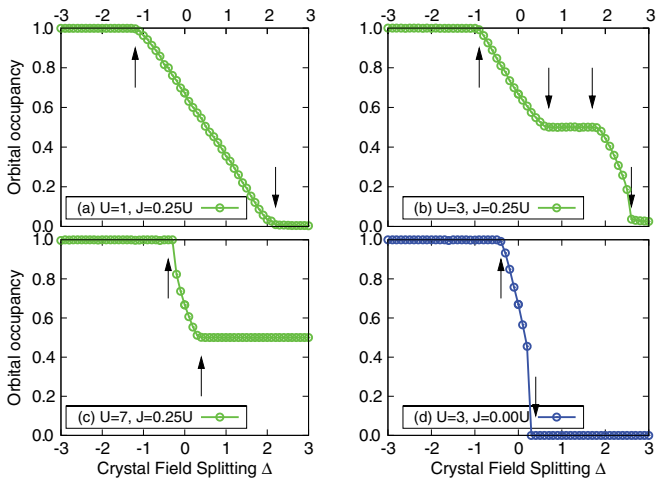

FIG. 5. (Color online) Orbital filling as a function of crystal field splitting Δ for selected Coulomb interaction U values. (a) $U = 1.0$. (b) $U = 3.0$. (c) $U = 7.0$. (d) $U = 3.0$. In (a)–(c), the interaction Hamiltonian is rotationally invariant with nonzero spin-flip and pair-hopping terms, whereas in (d) the interaction Hamiltonian is in the SU(N) scheme with $J = 0$. All the calculations are done by the DMFT + CT-HYB method[27,28] at finite temperature $T = 0.01$. Only the charge densities of the nondegenerate a_{1g} band are shown. The arrows correspond to phase-transition points.

The redistribution of the electrons among the three orbitals is the key point for the OSMT in this system and can be understood by the subtle effect of Hund's rule coupling, which favors the HS state with the (3,1) configuration. As for the SU(N) $J = 0$ case, the redistribution of electrons is much easier to understand. As shown in Fig. 4(b), the correlation effect induced by the Coulomb interaction increases the occupation of the a_{1g} band for the $\Delta < 0$ case and decreases it for the $\Delta > 0$ case, which is consistent with the results obtained with the traditional Hartree-Fock mean-field method.

C. HS-LS transition

In this section, we focus on the magnetic properties of the three-band model during the phase transitions, which have been reported rarely in the literature. In Fig. 6 we plot the evolution of the mean instantaneous moment, which is defined as $M_{\text{eff}} = \sqrt{\langle S_z^2 \rangle} = \sqrt{\langle (n_\uparrow - n_\downarrow)^2 \rangle}$, as a function of the Coulomb interaction strength U with selected crystal field splitting Δ. Actually, since the interaction Hamiltonian is rotationally invariant and the spin-rotation symmetry is conserved by the CT-HYB impurity solver[27] and the RIGA method,[34] we can easily prove that $\langle S_z^2 \rangle = \langle S_x^2 \rangle = \langle S_y^2 \rangle = \langle S^2 \rangle / 3$. We find that although the overall behavior of $\sqrt{\langle S_z^2 \rangle}$ looks quite similar for positive and negative crystal field splitting, the underlying physics are very different for the two cases.

For the negative crystal field splitting ($\Delta < 0$), with the increase of the Coulomb interaction strength and Hund's rule coupling, the system is approaching the (2,2) configuration (two electrons in both the a_{1g} and e'_g bands). The HS state can be reached smoothly when the two electrons in the e'_g bands fall into the triplet state due to the Hund's rule coupling.

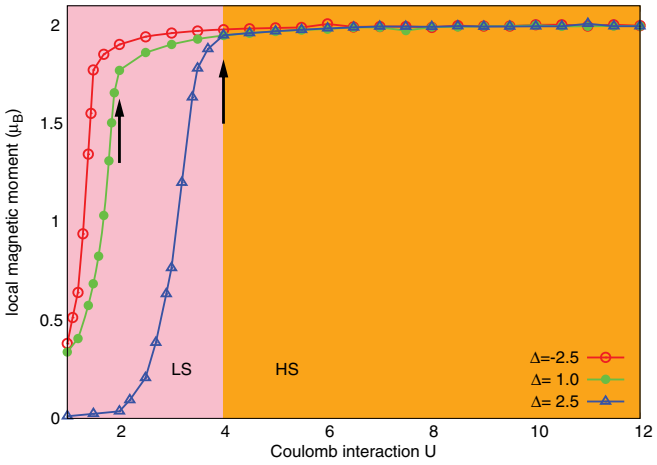

FIG. 6. (Color online) Calculated effective local magnetic moment $\sqrt{\langle S_z^2 \rangle}$ for the three-band Hubbard model with rotationally invariant interaction terms. The calculations are done with the DMFT + CT-HYB method[27,28] at finite temperature $T = 0.01$. Only the calculated results for representative crystal field splitting values ($\Delta = -2.5$, 1.0, and 2.5) are shown. The pink region denotes the LS phase, and the orange region denotes the HS phase. The arrows correspond to the possible phase-transition points.

Meanwhile, the Mott transition occurs when the spin state gets close to the HS state. Nevertheless, the situation for the positive crystal field splitting ($\Delta > 0$) is very different. Under weak Coulomb interaction, the occupation numbers of the system are closer to the (4,0) configuration (all four electrons are in the e_g' bands). With the increase of Coulomb interaction strength and Hund's rule coupling, when the crystal field splitting is still not strong enough to drive the system into the band insulator, the system undergoes two sequential transitions. The first transition is more related to the charge transfer from the e_g' bands to the a_{1g} band, and the system changes from the (4,0) to (3,1) configuration afterwards. This transition comes from the competition between the crystal field splitting, which favors the (4,0) configuration, and the Hund's rule coupling, which favors the (3,1) configuration. After the first transition, which manifests itself in Fig. 6 as a sharp upturn in the $\sqrt{\langle S_z^2 \rangle}$-$U$ curve for the $\Delta = 1.0$ case, the a_{1g} band is half-filled, and the e_g' bands are only quarter-filled. Since the system with half-filling is always much closer to a Mott transition,[5,20,21,26] the a_{1g} band becomes a Mott insulator first after the first transition, while the e_g' bands still remain metallic. A second transition occurs by further increasing the Coulomb interaction together with the Hund's rule coupling, after which the system becomes a Mott insulator for all the bands with the spin state being very close to a pure HS state.

IV. CONCLUDING REMARKS

In summary, we have studied the Mott transition in the three-band Hubbard model with orbital degeneracy lifting by crystal field splitting. By using the DMFT + CT-HYB method and the RIGA method, we have investigated how the orbital level splitting and the Hund's rule coupling affect the Mott transition in a system with four electrons per site. We obtain the following conclusions.

First, the Hund's rule coupling J (more specifically, the Ising-type Hund's rule coupling J_z) is the minimal requirement to induce OSMT and stabilize OSMP. In the phase diagram for the three-band Hubbard model with rotationally invariant interactions, the OSMP covers a wide parameter range. However, in the phase diagram for the three-band Hubbard model without any Hund's rule coupling terms, though the Mott MIT occurs when the Coulomb interaction strength reaches some critical value, the OSMP is totally absent.

Second, the interplay between the crystal field splitting and the Hund's rule coupling terms induces the redistribution of electrons among the three bands and leads to the complex phase diagrams. For example, the (4,0) charge configuration corresponds to a band insulator phase, the (3,1) charge configuration leads to an OSMP or Mott insulator phase, and the (2,2) charge configuration leads to a metal plus band insulator or Mott insulator plus band insulator phase.

Third, the appearance of the OSMP in this system is always accompanied by a HS-LS spin-state crossover. In the OSMP, the electronic distribution always remains in the (3,1) configuration, which strongly favors the HS state and lowers the Hund's rule energy. When the Coulomb interaction strength is reduced, the OSMP collapses to a metal phase accompanied by a HS-LS transition. Beyond that, in the metallic component of the OSMP, the non-Fermi-liquid feature is confirmed as well.

Finally, the three-band models arise in a number of other physically important contexts, including doped C_{60} and ruthenates and so on. In the present work, only the semicircular density of states is taken into account, which is oversimplified to understand the exotic physics generated by Hund's rule.[35] Extending our results to the models with a more realistic band structure is of high priority for future research.

ACKNOWLEDGMENTS

We acknowledge financial support from the National Science Foundation of China and from the 973 program of China under Contracts No. 2007CB925000 and No. 2011CBA00108. The DMFT + CT-HYB calculations have been performed on the SHENTENG7000 at the Supercomputing Center of the Chinese Academy of Sciences.

[1] M. Imada, A. Fujimori, and Y. Tokura, Rev. Mod. Phys. **70**, 1039 (1998).
[2] A. Georges, G. Kotliar, W. Krauth, and M. J. Rozenberg, Rev. Mod. Phys. **68**, 13 (1996).
[3] Y. Tokura and N. Nagaosa, Science **288**, 462 (2000).
[4] C.-K. Chan, P. Werner, and A. J. Millis, Phys. Rev. B **80**, 235114 (2009).
[5] P. Werner and A. J. Millis, Phys. Rev. Lett. **99**, 126405 (2007).
[6] V. I. Anisimov, I. A. Nekrasov, D. E. Kondakov, T. M. Rice, and M. Sigrist, Eur. Phys. J. B **25**, 191 (2002).

[7]G. Kotliar, S. Y. Savrasov, K. Haule, V. S. Oudovenko, O. Parcollet, and C. A. Marianetti, Rev. Mod. Phys. **78**, 865 (2006).
[8]S. Florens, A. Georges, G. Kotliar, and O. Parcollet, Phys. Rev. B **66**, 205102 (2002).
[9]A. O. Shorikov, Z. V. Pchelkina, V. I. Anisimov, S. L. Skornyakov, and M. A. Korotin, Phys. Rev. B **82**, 195101 (2010).
[10]J. Kunes, A. V. Lukoyanov, V. I. Anisimov, R. T. Scalettar, and W. E. Pickett, Nat. Mater. **7**, 198 (2008).
[11]L. Craco, M. S. Laad, and E. Müller-Hartmann, Phys. Rev. B **74**, 064425 (2006).
[12]A. Koga, N. Kawakami, T. M. Rice, and M. Sigrist, Phys. Rev. Lett. **92**, 216402 (2004).
[13]A. Koga, N. Kawakami, T. M. Rice, and M. Sigrist, Phys. Rev. B **72**, 045128 (2005).
[14]A. Liebsch, Phys. Rev. Lett. **91**, 226401 (2003).
[15]A. Liebsch, Phys. Rev. B **70**, 165103 (2004).
[16]C. Knecht, N. Blümer, and P. G. J. van Dongen, Phys. Rev. B **72**, 081103 (2005).
[17]R. Arita and K. Held, Phys. Rev. B **72**, 201102 (2005).
[18]P. G. J. van Dongen, C. Knecht, and N. Blümer, Phys. Status Solidi B **243**, 116 (2006).
[19]M. Ferrero, F. Becca, M. Fabrizio, and M. Capone, Phys. Rev. B **72**, 205126 (2005).
[20]P. Werner, E. Gull, and A. J. Millis, Phys. Rev. B **79**, 115119 (2009).
[21]E. Jakobi, N. Blümer, and P. van Dongen, Phys. Rev. B **80**, 115109 (2009).
[22]M. Neupane, P. Richard, Z.-H. Pan, Y.-M. Xu, R. Jin, D. Mandrus, X. Dai, Z. Fang, Z. Wang, and H. Ding, Phys. Rev. Lett. **103**, 097001 (2009).
[23]L. de' Medici, S. R. Hassan, M. Capone, and X. Dai, Phys. Rev. Lett. **102**, 126401 (2009).
[24]L. de'Medici, A. Georges, and S. Biermann, Phys. Rev. B **72**, 205124 (2005).
[25]J. Bnemann, D. Rasch, and F. Gebhard, J. Phys. Condens. Matter **19**, 436206 (2007).
[26]T. Kita, T. Ohashi, and N. Kawakami, Phys. Rev. B **84**, 195130 (2011).
[27]P. Werner and A. J. Millis, Phys. Rev. B **74**, 155107 (2006).
[28]P. Werner, A. Comanac, L. de' Medici, M. Troyer, and A. J. Millis, Phys. Rev. Lett. **97**, 076405 (2006).
[29]E. Gull, A. J. Millis, A. I. Lichtenstein, A. N. Rubtsov, M. Troyer, and P. Werner, Rev. Mod. Phys. **83**, 349 (2011).
[30]E. Gull, P. Werner, S. Fuchs, B. Surer, T. Pruschke, and M. Troyer, Comput. Phys. Commun. **182**, 1078 (2011).
[31]J. Bünemann, W. Weber, and F. Gebhard, Phys. Rev. B **57**, 6896 (1998).
[32]J. Bünemann, F. Gebhard, T. Ohm, S. Weiser, and W. Weber, Phys. Rev. Lett. **101**, 236404 (2008).
[33]X. Y. Deng, L. Wang, X. Dai, and Z. Fang, Phys. Rev. B **79**, 075114 (2009).
[34]N. Lanatà, H. U. R. Strand, X. Dai, and B. Hellsing, Phys. Rev. B **85**, 035133 (2012).
[35]L. de' Medici, J. Mravlje, and A. Georges, Phys. Rev. Lett. **107**, 256401 (2011).